Available online at www.sciencedirect.com
SCIENCE DIRECT®
Journal of Sound and Vibration 291 (2006) 1–18
JOURNAL OF SOUND AND VIBRATION
www.elsevier.com/locate/jsvi

Experimental study of stick-slip dynamics in a friction wedge damper

N.K. Chandiramani*, K. Srinivasan, J. Nagendra

Department of Mechanical Engineering, Indian Institute of Technology, Guwahati 781039, India

Received 15 May 2004; received in revised form 21 December 2004; accepted 23 May 2005
Available online 19 August 2005

Abstract

Investigations are performed on a friction wedge damper model with the objective of studying stick-slip phenomena at various excitation frequencies. Model design considerations include maintaining dry friction sliding-contact and near-vertical motion. Time traces, phase portraits and frequency spectra are presented for the relative displacement and velocity. Stick-slip phenomena, found to be characterized by harmonic distortions, appear consistently in the vicinity of 30 Hz and less so at higher frequencies. There appears to be a transition from stick-slip to pure-slip motion between 30 and 40 Hz. This transition is characterized by a sharp increase in peak-to-peak response. Two types of stick-slip phenomena, distinguishable by the direction of relative velocity before and after stick, are observed.

1. Introduction

Friction wedges are used in railroad vehicles as damping elements in the suspension system. They dissipate energy arising from motion over undulating rails. Their popularity is due to their simple construction, reliability during operation, and low running costs.

Xia [1] considered wedge dampers involving two-dimensional dry friction. One interesting phenomenon observed is that a lateral exciting force on the bolster will cause both lateral as well as vertical vibrations of the wedge and the bolster. Shaw [2] considered a single degree of freedom

*Corresponding author. Tel.: +91 361 2582090; fax: +91 361 2690762.
E-mail address: naresh@iitg.ernet.in (N.K. Chandiramani).

0022-460X/$ - see front matter © 2005 Elsevier Ltd. All rights reserved.
doi:10.1016/j.jsv.2005.05.024

system with dry friction and determined the asymptotic stability of steady-state motions. For positive viscous damping, the non-sticking steady-state solutions with period equal to the forcing period were shown to be almost always asymptotically stable. For negative viscous damping such solutions become unstable. The possibility of aperiodic motions containing two incommensurate frequency components was demonstrated. Anderson and Ferri [3] considered a system with combined viscous and dry friction damping, the latter having constant, velocity-dependent, and displacement-dependent components. It was seen that under certain conditions, the displacement-dependent friction gives rise to viscous-damping like characteristic. The response amplitude could also increase by addition of displacement-dependent friction. Narayanan and Jayaraman [4] considered dry friction with cubic stiffness and viscous damping and obtained a sequence of period doubling bifurcations and chaos.

Feeny and Moon [5] studied, experimentally and numerically, the chaotic dynamics of a harmonically forced spring-mass system with dry friction. The friction in the experiment was designed to vary linearly with displacement. Three friction models are used in the simulations, i.e., Coulomb model, continuous model, and a state-variable model. Using experimental Poincaré maps, the qualitative features of the chaotic attractor in three-dimensional phase space were obtained and were used to evaluate the applicability of the three friction models. The state-variable model was found to closely match the experimental data. Hinrichs et al. [6] investigated the dynamics of a friction oscillator under self and external excitation. The rich bifurcational behaviour predicted by numerical simulations is compared with experimental results. A detailed look at the non-smooth transition points of the experimental trajectories showed that a refined friction model is required. Hence, a bristle model, i.e., friction contact with tangential stiffness and damping, and a stochastic friction model were proposed. Kaiser et al. [7] proposed a model for the friction wedge damper used in rail cars. Steady-state responses were obtained using various friction laws and parameterizations in track frequency and amplitude. They also reported stick-slip response, indicating strong nonlinearity, for small track amplitudes and sub-resonant track frequencies. However at larger amplitudes and frequencies, sticking was absent.

To the authors' knowledge, there has been no experimental study reported on stick-slip phenomena in friction wedge damper configurations of practical importance. Hence, in the present work, experimental studies are performed on the model (Fig. 1) considered by Kaiser et al. [1], that finds applications in railcars. The geometric and kinematic parameters used in the fabrication are adapted from their work. The objective of the study is to detect stick-slip motion for a range of excitation frequencies and establish a correspondence between occurrences of stick-slip and excitation frequencies.

2. Mechanical model of friction wedge suspension system

Fig. 1 shows the schematic of the experimental model of a friction wedge damper. The payload weight acts on the bolster. The bolster and friction wedges are suspended on the side-frame via spring nests. Dry friction sliding contact exists between the bolster and the wedge, as well as between the wedge and the side-frame wall. Symmetry of the model and its motion—about the central vertical plane—is implied. The variables X and Y denote horizontal and vertical displacements, respectively. The side-frame is rigidly mounted on the exciter and hence its

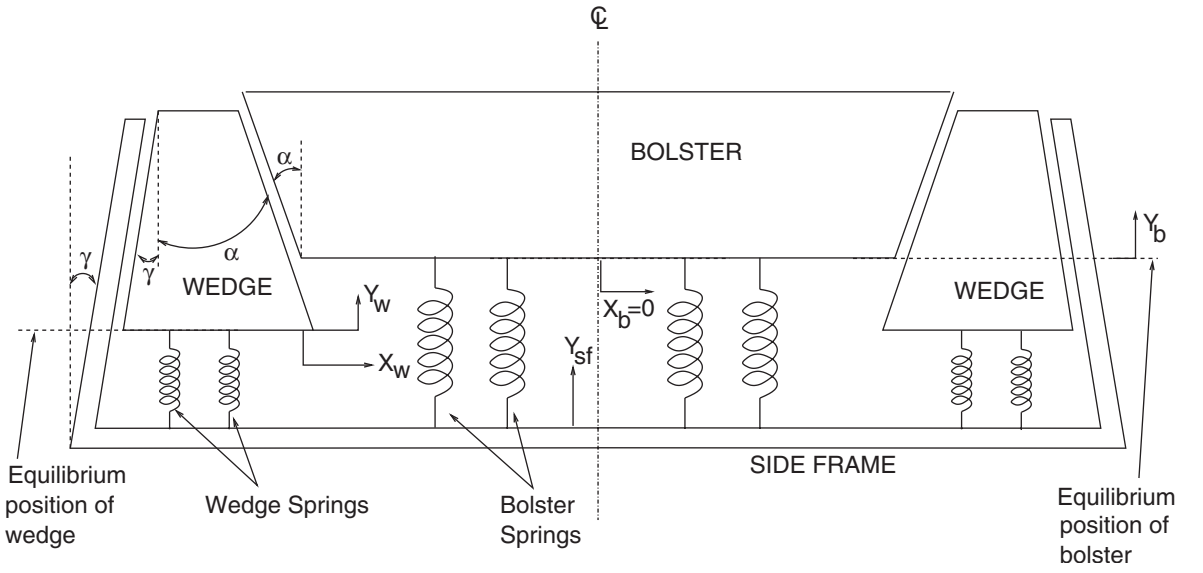

Fig. 1. Schematic of the friction wedge damper model.

displacement (Y_{sf}) equals that of the exciter. This models track undulations that are transmitted directly to the side-frame. The displacements of the bolster (Y_b) and the wedge (Y_w) are measured with respect to the point on the side-frame corresponding to the equilibrium position of bolster and wedge, respectively. In order to ensure that dry friction contact is always maintained during operation at all the sliding contact surfaces, the wedge springs are provided with sufficient precompression and then tucked under the bolster during assembly. The initial precompression of wedge and bolster springs are denoted as Y_{b0} and Y_{w0} (positive upward), respectively. A periodic excitation of amplitude A and frequency ω is applied to the side-frame. Due to symmetry of motion and contact at sliding interfaces being maintained, the model vibrates as an SDOF system, with the bolster displacement being sufficient to define the system configuration. This fact is exploited in the present experiment and hence only the vertical displacements of bolster and side-frame were measured.

When considering the Coulomb model, the friction force (F) is given by $F = \mu N \operatorname{sgn}[\dot{y}]$ for $\dot{y} \neq 0$ and $-\mu N \leqslant F \leqslant \mu N$ for $\dot{y} = 0$. Here N, μ, and $\dot{y}$ denote normal force, friction coefficient, and relative sliding velocity, respectively, between the contact surfaces. The friction coefficient is given by $\mu = \mu_k$ for $\dot{y} \neq 0$, and $\mu = \mu_s$ for $\dot{y} = 0$, $\mu_k \leqslant \mu_s$. Hence, the Coulomb model yields a discontinuous and multivalued friction force, when $\dot{y} = 0$, which causes stick-slip motion to occur. The bolster and wedge masses, and wedge and side-frame angles are M_b and M_w, and α and γ, respectively. A sinusoidal track undulation $Y_{sf} = A_T \cos[\Omega t]$ is assumed. The condition of permanent contact between adjacent sliding faces results in the constraints $X_w = \tan[\gamma] Y_w$, $Y_w = \Gamma Y_b$, where $\Gamma = \tan[\alpha]/(\tan[\alpha] + \tan[\gamma])$. Considering the dynamic equilibrium of the wedge in the horizontal and vertical directions and the bolster in the vertical direction, and using the constraints to eliminate the X_w and Y_w, the non-dimensional equation of motion is obtained as [7]

$$\ddot{y} + F^{\pm} y + H^{\pm} + G^{\pm}[1 - a\beta^2 \cos(\beta\tau)] = 0, \tag{1}$$

where y, β, a, and τ are dimensionless bolster displacement ($y = (\omega^2/g)Y_b$), track frequency ($\beta = \Omega/\omega$), track amplitude ($a = (\omega^2/g)A_T$), and time ($\tau = \omega t$), respectively, where $\omega^2 = K_b/M_b$. The coefficients F, G, H, (detailed in Ref. [7]) contain the term $\mathrm{sgn}[\dot{y}]$ arising from the Coulomb friction law. They are functions of the suspension model parameters, i.e., geometry (wedge and side-frame angles), masses of wedge and bolster, stiffnesses (K_w, K_b) and pre-compressions of wedge and bolster spring nests, and friction coefficient at sliding interfaces. Due to the $\mathrm{sgn}[\dot{y}]$ term, F, G, H are constant but discontinuous across the zero-velocity plane, i.e., the $(+)$ superscripted quantities valid for upward motion of the bolster (i.e., $\mathrm{sgn}[\dot{y}] = 1$) differ from their $(-)$ superscripted counterparts that correspond to downward motion of the bolster (i.e., $\mathrm{sgn}[\dot{y}] = -1$). Thus Eq. (1) is non-smooth and yields stick-slip motions. The variation—during each cycle of motion—of the normal forces (and hence the friction forces) at the contact faces is included in Eq. (1).

3. Fabrication of the experimental model

During fabrication, the suspension model parameters (as noted above) were appropriately chosen so as to ensure that (a) the values of the non-dimensionalized quantities F, G, H, are comparable to those considered in Ref. [7], (b) the kinematic constraint, i.e., no loss of contact at sliding interfaces, is maintained, (c) the masses and springs undergo near-vertical translation only. Based on the capacity of the exciter, the total mass of the model was chosen as 1.5 kg. Using the total mass and the measured friction coefficient, the individual masses of the bolster, wedge, and side-frame, and the stiffnesses of the bolster and wedge spring nests were obtained such that suitable values of F, G, H, result, as noted above. Table 1 shows the values of the design parameters of the present experimental model, and Table 2 compares the non-dimensional parameters obtained for the present model with those used in the simulations in Ref. [7].

The model was fabricated out of perspex since it is light and affords easy machinability. Fig. 2 shows a photograph of the model. The side walls and bottom plate of the side-frame were rigidly fastened so as to provide strength for withstanding the large dynamic forces that occur during experimentation. In order to eliminate the lateral motion of the bolster and wedges, i.e., to

Table 1
Parameters of the experimental model

Parameter	Value
Mass of each wedge (M_w)	0.17 kg
Mass of bolster (M_b)	0.7 kg
Effective stiffness of each wedge group of springs (K_w)	2550.6 N/m
Effective stiffness of bolster group of springs (K_b)	5101.2 N/m
Wedge angle (α)	37.5°
Side frame angle (γ)	4°
Friction coefficient at all sliding interfaces	0.29
Offset of wedge springs (pre-compression) (Y_{w0})	−3.46 mm
Offset of bolster springs (pre-tension) (Y_{b0})	3.04 mm

Table 2
Comparison of non-dimensional parameters of the present work with those of Kaiser et al. [7]

Source	F^+	F^-	G^+	G^-	H^+	H^-
Present work	1.1918	1.3735	1.0122	1.0369	0.7561	−0.5237
Kaiser et al. [7]	1.0357	1.0368	1.0000	1.0001	−1.5035	−1.5494

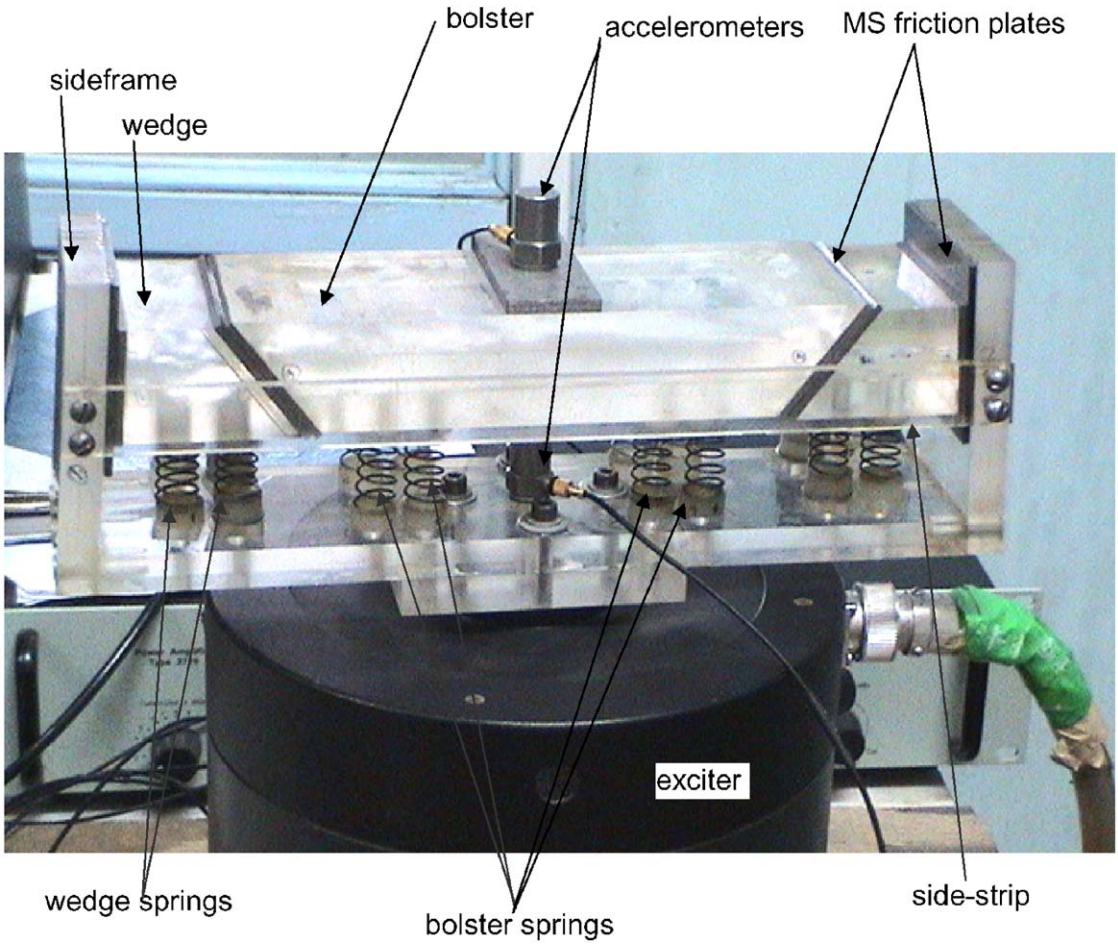

Fig. 2. Photograph of the model.

maintain one-dimensional (vertical) motion of the model, two rows of springs were provided laterally. Further, thin side-strips of highly polished perspex were fastened to the two lateral faces of the side-frame such that lateral motions are arrested within 0.5 mm. Thus, the occasional contact occurring between wedge/bolster and the side-strip is almost frictionless. The side-frame, wedges, and bolster contain holes for fixing the springs. The ends of the springs were mounted in

the recesses of nylon caps, using epoxy resin. The caps were then interference-fitted into the holes on the side-frame, bolster and wedges.

If perspex is used at the wedge–side-frame and the wedge–bolster interfaces, due to the fact that perspex is diamagnetic, large static charges develop during the sliding contact that occurs at these interfaces. This results in unusually high friction coefficients that were not determinable consistently. Hence machined plates made of mild steel were used as the sliding friction surfaces by mounting them on to the perspex components. Another advantage of using mild steel at sliding interfaces is the surface uniformity attainable during grinding, which ensures that the friction coefficient is constant over the plate. The friction coefficient between pairs of contacting mild steel plates is measured using the standard inclined plane apparatus. During model assembly, as mentioned earlier, the wedges are forcibly tucked under the bolster in a manner such that they reside in the gap between side-frame and bolster. This provides the required pre-compression to prevent loss of contact along sliding faces during excitation. The normal force (and hence friction force) varies during the period of motion.

4. Experimental procedure

Since the experimental setup is designed to behave as a SDOF system, the dynamics of relative motion between the bolster and the side-frame is studied. The experimental setup comprises: (i) the friction wedge damper model being investigated, (ii) excitation mechanism, and (iii) instrumentation and analysis setup. The excitation part of the setup consists of a function generator, a power amplifier and an exciter, connected in that order. The instrumentation setup consists of one accelerometer each mounted on bolster and side-frame, measuring amplifier, differencing circuit, signal conditioning module and oscilloscope. The experimental layout is shown in Fig. 3. A B&K type 4808 electromagnetic exciter was used in conjunction with a B&K

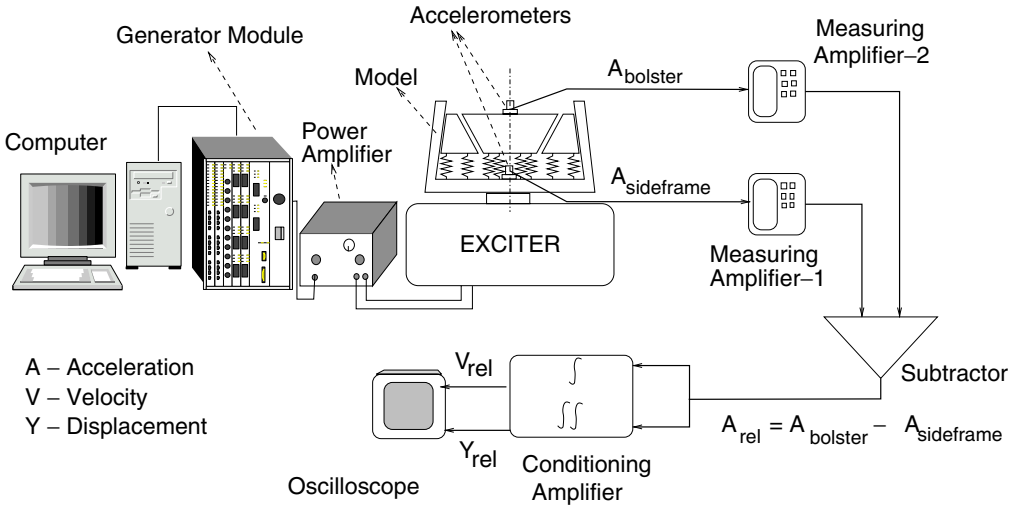

Fig. 3. Layout of experimental setup.

power amplifier type 2706. Input to the power amplifier comes from a function generator (i.e., the generator module of B&K Pulse 2825). The signal generator module is controlled using B&K Pulse 3560 software so as to obtain various excitation signals. Amplifier gain settings were used for adjusting the RMS output current through which the output power can be varied in order to adjust the excitation amplitude. In this manner the loss in excitation amplitude, that occurs when increasing excitation frequency, was compensated. This yields a constant amplitude excitation as measured by the side-frame accelerometer. A calibration table of gain settings versus excitation frequency, thus prepared, was used for obtaining constant amplitude excitation.

Accelerometers of ICP type (B&K 4396) were used. They were connected to measuring amplifiers (B&K type 2525), which acted as power supplies for the accelerometers and also amplified the acceleration signals tenfold. These amplified signals were fed to the differencing circuit comprising an op-amp (Fig. 4). The two signals to be differenced, i.e., bolster and side-frame accelerometer signals, are V_1 and V_2, respectively. The value of resistors is $R_1 = R_2 = 10\,\mathrm{k\Omega}$, $R_f = 100\,\mathrm{k\Omega}$. Hence the output at terminal-3 is $10(V_2 - V_1)$. The output from terminal-3 was fed via a T-connector to the two input channels of the conditioning amplifier (B&K model 2963). The inputs were band-pass filtered in the range 1 Hz–10 kHz. Subsequently, one of the inputs was integrated once, and the other was double integrated. The outputs from the conditioning amplifier were fed to a two channel digital storage oscilloscope (DSO, Agilent 54622D) for analysis. Both time and frequency domain analyses were performed. Phase portraits depicting the relative bolster–side-frame velocity versus the corresponding displacement were obtained. In order to minimize noise, the signals were averaged using standard options in the DSO.

Poincaré sections were obtained for determining whether the response is periodic or not. The external trigger channel of the DSO was used for this purpose. When the voltage input to this channel is below 1.4 V, the phase space is displayed, otherwise the display is suppressed by the trigger. An arbitrary function generator (Tektronix AFG320) was used to generate the triggering signal to the trigger channel of the DSO. The signal is generated so as to remain below 1.4 V for small time intervals, with these intervals pulsed at the side-frame's excitation frequency. Hence, a sharp point is obtained on the screen. The motion is termed n-periodic when n distinct points are obtained on the display, i.e., the response period is n times that of excitation. However, experimental Poincaré sections revealed only period-1 motion.

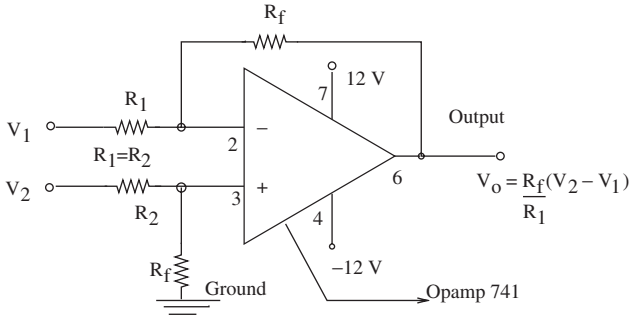

Fig. 4. Differencing circuit to obtain relative motion.

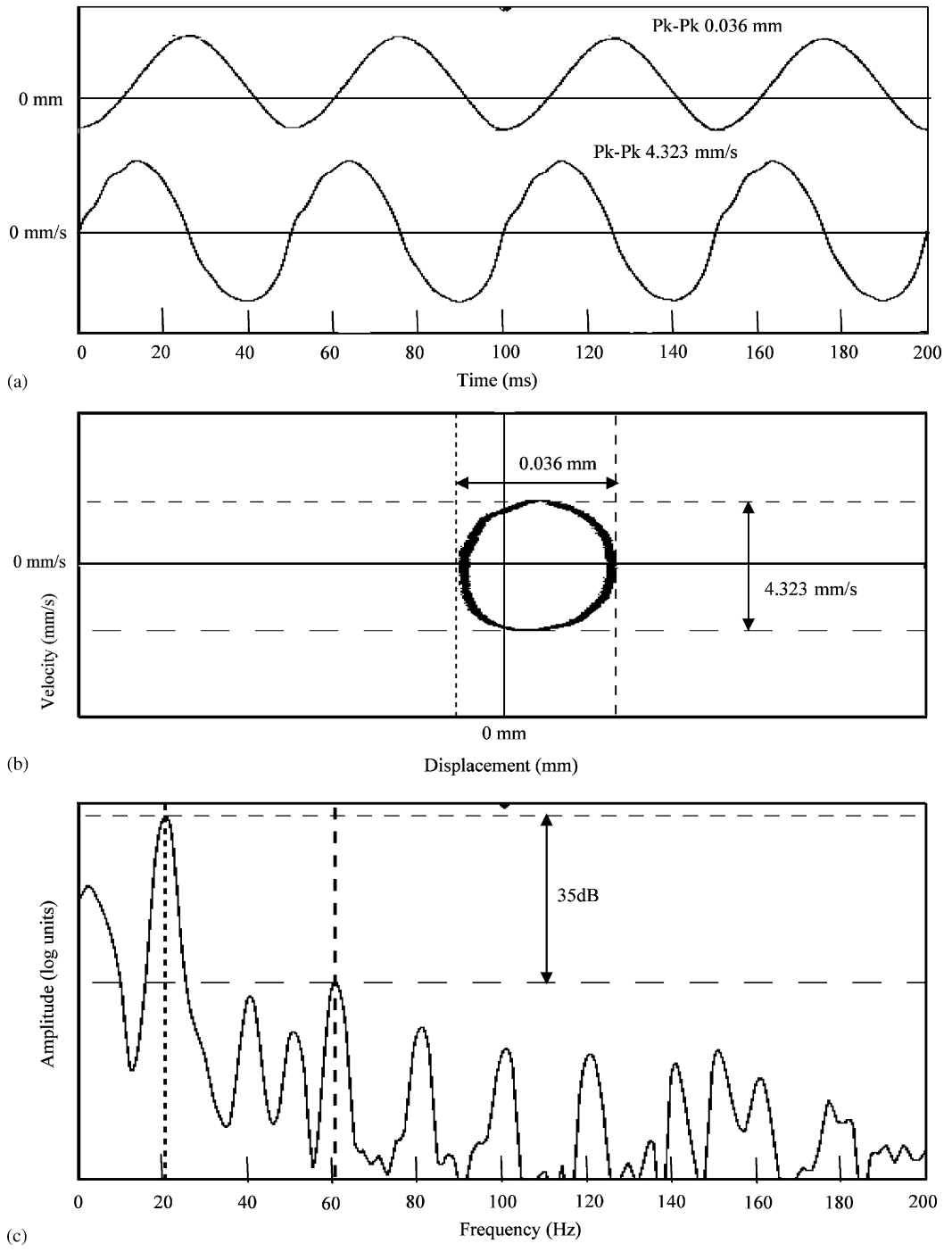

Fig. 5. Time traces (a), phase portrait (b), FFT (c) of the relative motion, 20 Hz excitation.

5. Results and discussion

The excitation signals are purely sinusoidal with frequency (ω) varied from 20 to 40 Hz in steps of 0.5 Hz. Time traces of the relative-displacement and the relative-velocity, phase portraits, and FFTs of the relative-displacement have been obtained for studying the stick-slip behaviour. These are displayed as parts (a), (b), and (c), respectively, in the figure corresponding to a particular excitation frequency. Results are presented for few representative frequencies (20, 25, 28.5, 29, 29.5, 30, and 40 Hz) at which stick-slip is absent or dominant. Stick-slip oscillations are characterized by time intervals during which the relative-displacement is constant, i.e., the relative-velocity is zero. However, while stick-slip appears in non-smooth dynamical systems, such behaviour is difficult to realize experimentally since the Coulomb model is an idealization of the more realistic continuous friction model which approximates the discontinuity by using a hyperbolic secant–tangent function [5]. Thus, the experimental results displayed correspond to near-stick-slip oscillations. Stick events are encircled in the respective time traces and phase portraits.

Fig. 5 shows the results for an excitation frequency of 20 Hz. The relative motion is evidently periodic, with a sinusoidal-like relative-displacement. Since there appears no interval during which the relative-displacement remains constant, one can infer the absence of sticking events. This is also evident from the oval-like phase portrait. The FFT shows a peak at the excitation frequency of 20 Hz. The amplitude of the second, third, and fourth harmonics are 38.4, 35, and 44.66 dB, respectively, below that of the fundamental. The corresponding amplitude ratios (AR), referenced to the fundamental, are 1/83.18, 1/56.23, and 1/171, respectively. Hence we can conclude that the system exhibits a weak cubic and quadratic nonlinearity. Table 3 shows the details of the amplitudes of higher harmonics relative to that of the fundamental. The comparison is shown both in terms of dB differences (ΔdB) and AR for the second, third, and fourth highest peaks. Here, h_n denotes the harmonic number corresponding to these peaks. Results for an excitation at 25 Hz, are shown in Fig. 6. The increased effect of quadratic and cubic nonlinearity is evidenced by the relatively stronger peaks corresponding to the second, third, and fourth harmonics (Fig. 6(c) and Table 3). This is also apparent from the harmonic distortions present in the relative-velocity time trace (Fig. 6(a)) and the phase portrait (Fig. 6(b)).

Table 3
Amplitudes of higher harmonics relative to the fundamental: ΔdB (dB difference, fundamental—harmonic), AR (amplitude ratio, fundamental:harmonic), h_n (harmonic number)

Exc. freq. (Hz)	Second highest peak			Third highest peak			Fourth highest peak		
	ΔdB	AR	h_n	ΔdB	AR	h_n	ΔdB	AR	h_n
20	35	56.2	3	38.4	83.2	2	44.7	171.8	4
25	28.1	25.4	2	31.5	37.5	3	39.9	98.9	4
28.5	18.8	8.7	2	24.2	16.2	3	25.2	18.3	4,5
29	19.1	9	3	22.3	13	5	26.1	20.1	4
29.5	17.3	7.3	3	24	15.8	2,4,5	31.9	39.5	6
30	18.8	8.7	3	21.1	11.3	2	24.8	17.4	5
40	18.8	8.7	2	32	39.8	3	36.8	69.5	4

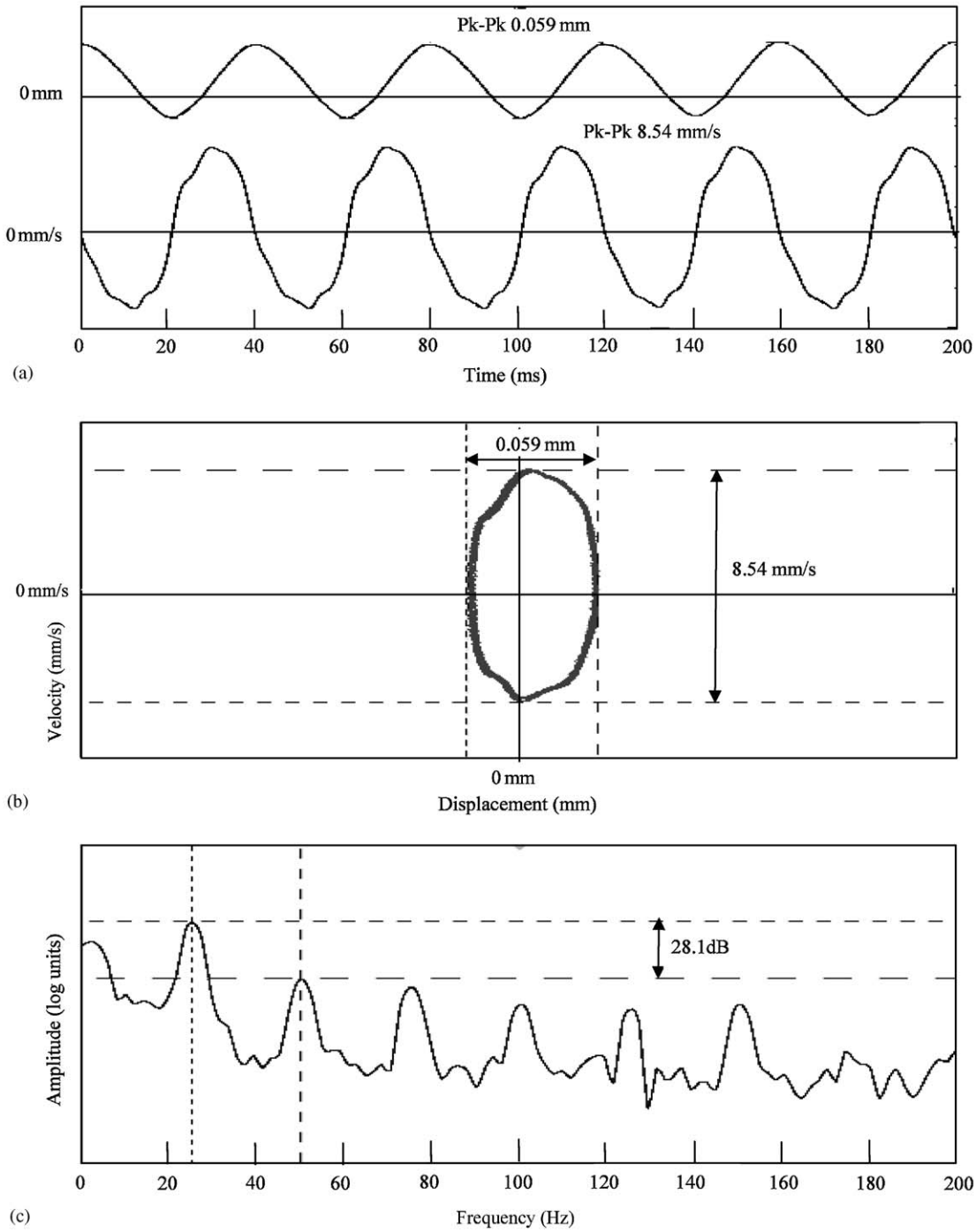

Fig. 6. Time traces (a), phase portrait (b), FFT (c) of the relative motion, 25 Hz excitation.

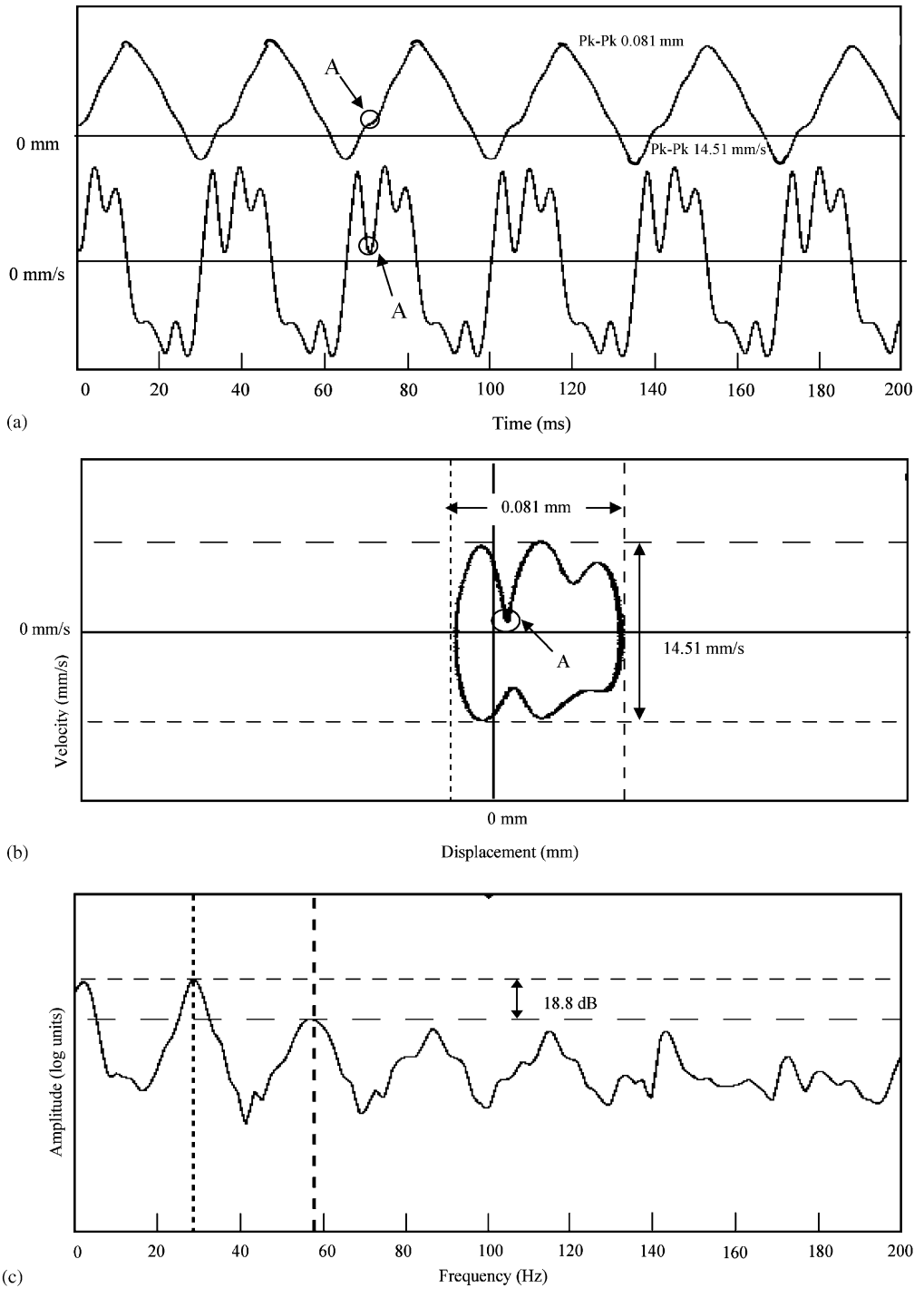

Fig. 7. Time traces (a), phase portrait (b), FFT (c) of the relative motion, 28.5 Hz excitation.

The first occurrence of near-stick behaviour is for an excitation of 28.5 Hz, as shown in Fig. 7. The relative displacement is almost constant for around 2 ms (stick duration) per cycle, during which the relative velocity remains almost zero. This near-stick event is characterized by the direction of the velocity being same just before and just after the stick event, i.e., the velocity trace as well as the orbit in the phase portrait almost touch the zero velocity line. This is termed type-A stick-slip (see Fig. 8). Only one stick occurs per cycle of motion. The velocity trace shows a prominence of higher harmonics and this distortion is also visible in the phase portrait and the frequency spectrum. The latter shows that the higher harmonics have relatively larger amplitudes as compared to the results for 20 and 25 Hz, for which sticking did not occur (see also Table 3). This is also evident in the remaining cases that exhibit stick events. The results for excitation frequencies of 29 Hz (Fig. 9) and 29.5 Hz (Fig. 10) reveal type-A stick-slip with stick duration of around 3.5 ms per cycle (i.e., one stick event per cycle). For an excitation frequency of 30 Hz, type-A stick-slip occurs with stick duration of around 2 ms, as indicated in Fig. 11. In addition, type-B stick-slip—characterized by the relative velocity remaining zero and then reversing direction (Fig. 8)—occurs with stick duration of around 3.5 ms per cycle. Thus, there are two stick events per cycle at 30 Hz excitation.

Stick events were not regularly obtained at frequencies beyond 30 Hz. Hence, the frequency range between 30 and 40 Hz appears to be a transition from stick-slip to pure slip. For example, at 40 Hz, type-B stick-slip was observed as displayed in Fig. 12. This transitory behaviour conforms to numerical results of Kaiser et al. [7] who reported pure slip motions at higher excitation frequencies. Fig. 13 shows the peak-to-peak relative displacement and relative velocity versus excitation frequency. There appears a sharp increase in the peak-to-peak values beyond 35.5 Hz, thus indicating the predominance of slip over stick, and thereby conforming to the aforementioned transitory behaviour observed between 30 and 40 Hz region. This increasing relative motion between bolster and side-frame conforms to the frequency response numerically obtained by Kaiser et al. [7], wherein the system behaves like a weakly damped SDOF linear oscillator. The experimentation was stopped at 40 Hz since the model began undergoing large relative motions beyond 40 Hz due to which the contact at interfaces was being intermittently lost, i.e., an impact-cum-friction oscillator system arose beyond 40 Hz.

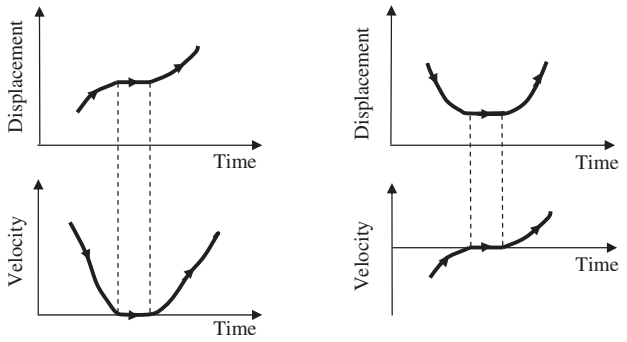

Fig. 8. Schematic of time traces corresponding to types-A and -B stick behaviour.

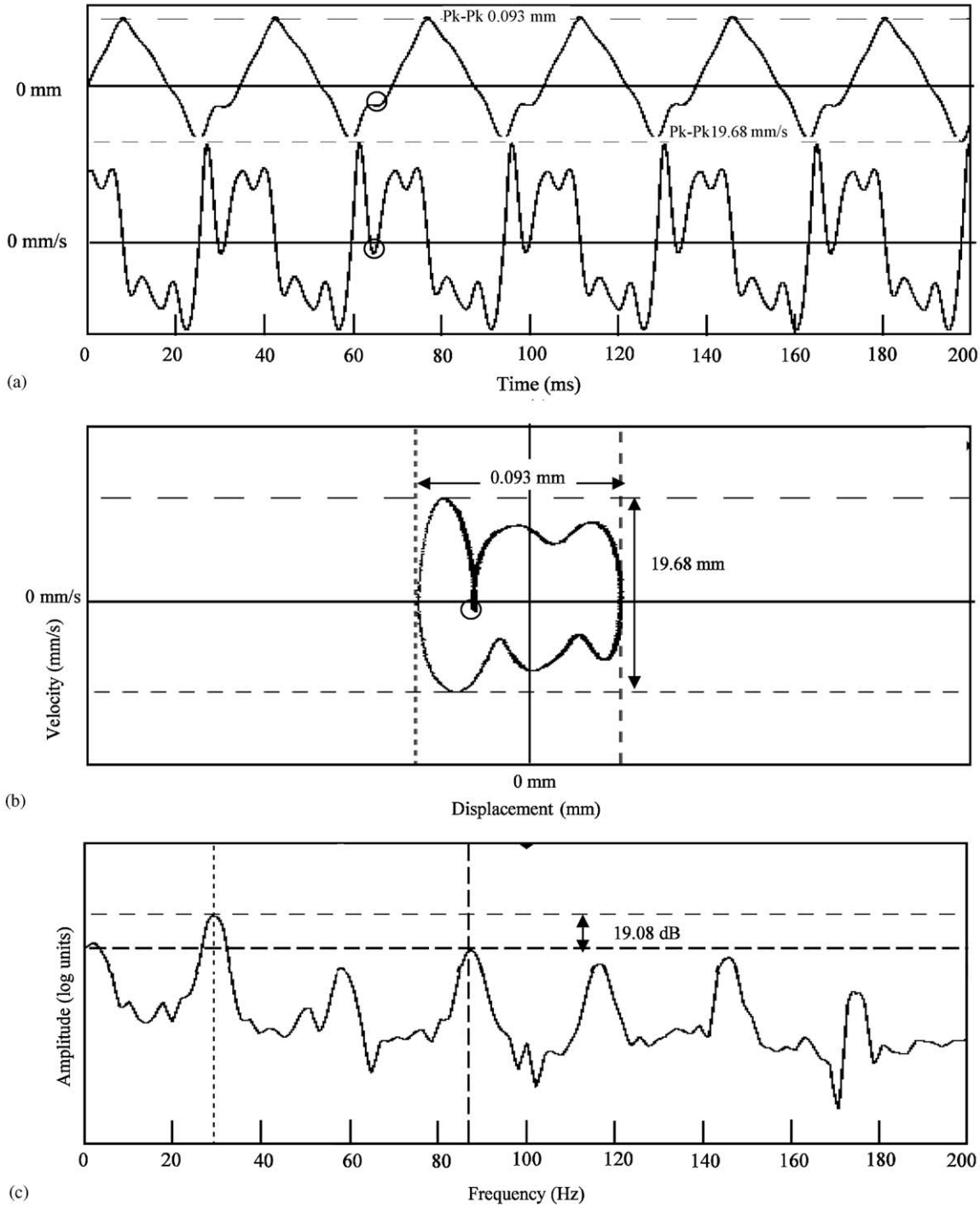

Fig. 9. Time traces (a), phase portrait (b), FFT (c) of the relative motion, 29 Hz excitation.

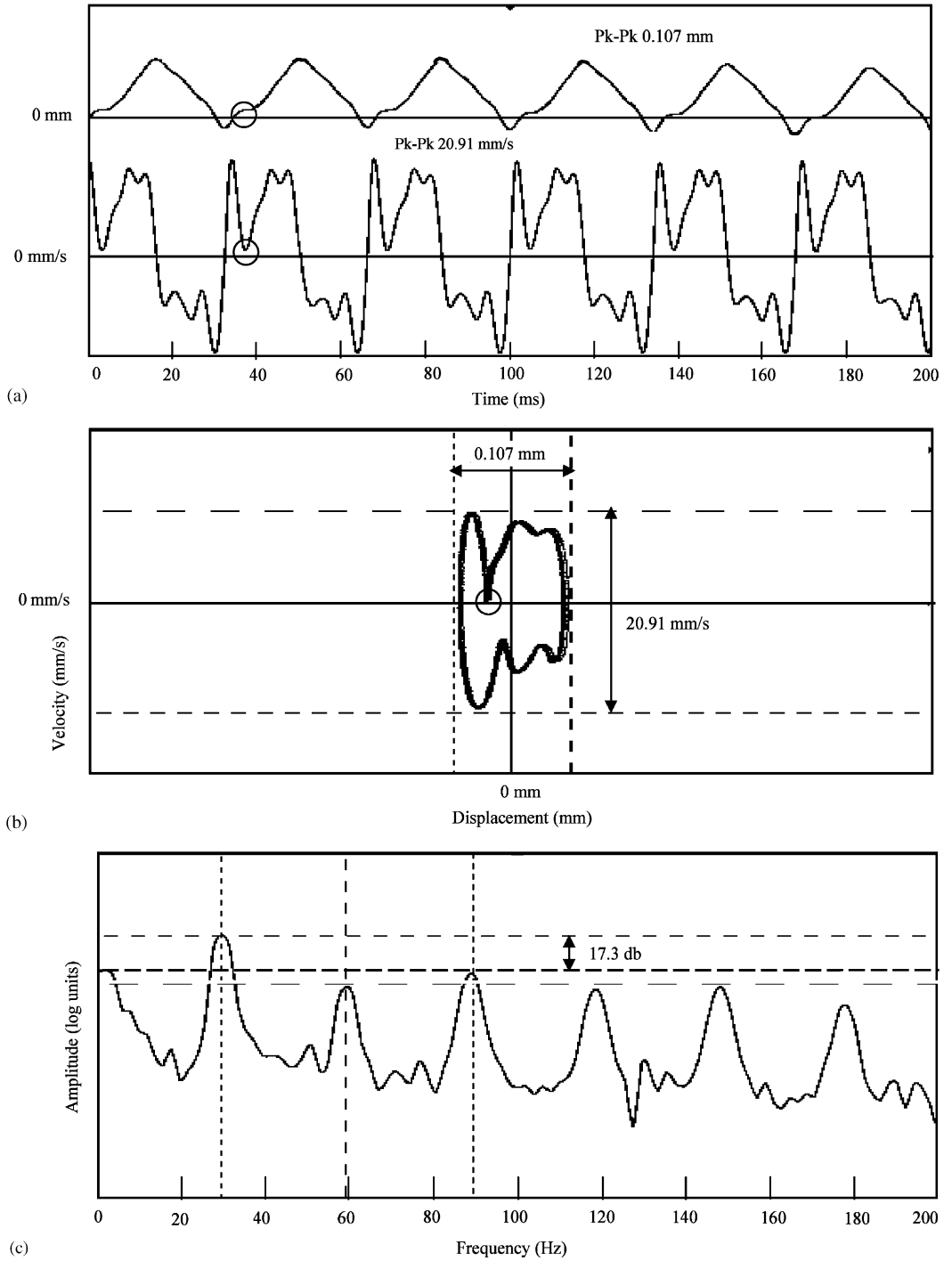

Fig. 10. Time traces (a), phase portrait (b), FFT (c) of the relative motion, 29.5 Hz excitation.

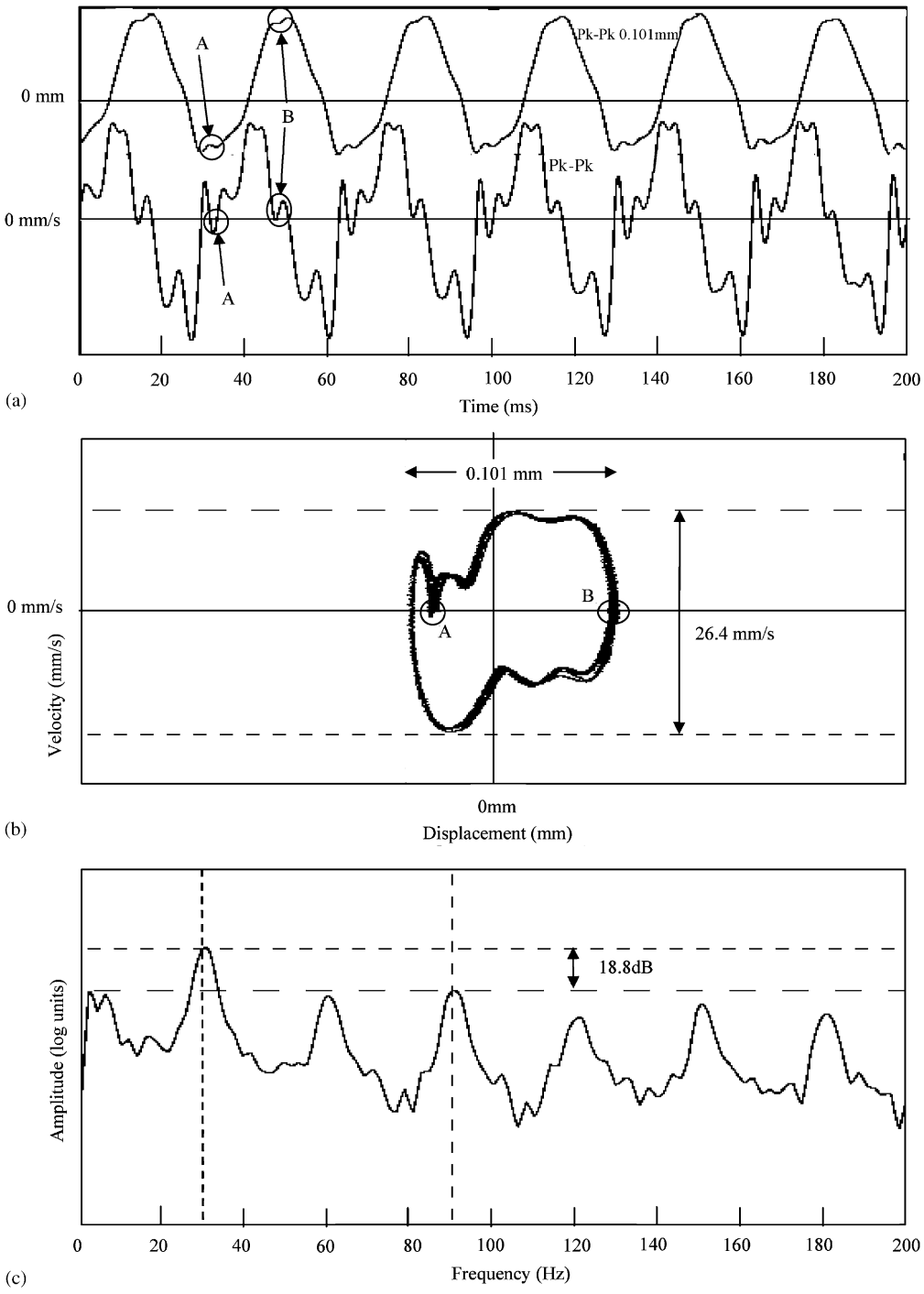

Fig. 11. Time traces (a), phase portrait (b), FFT (c) of the relative motion, 30 Hz excitation.

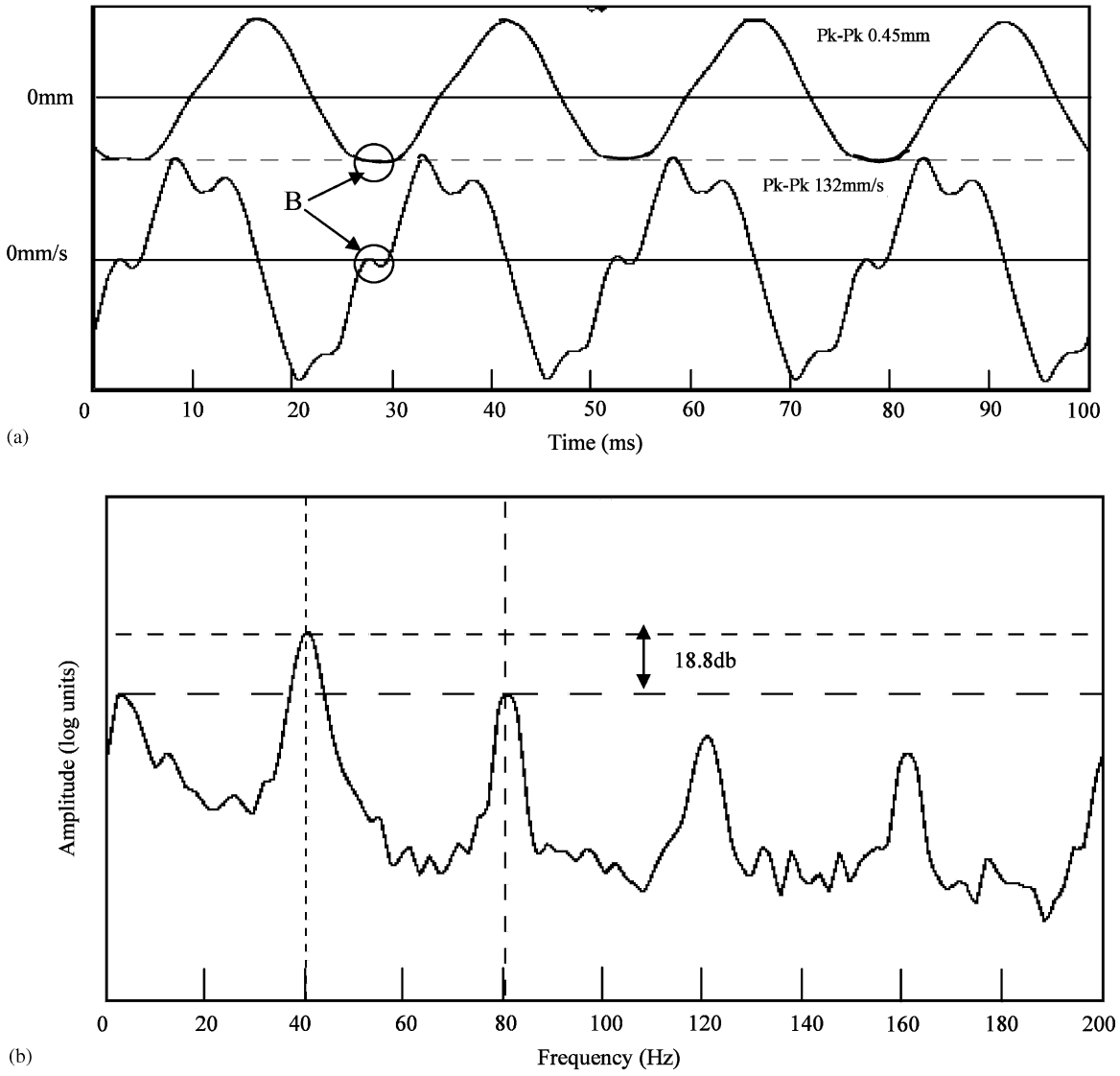

Fig. 12. Time traces (a), FFT (b) of the relative motion, 40 Hz excitation.

6. Summary and conclusions

A SDOF friction wedge damper model was designed in compliance with the analytical model considered in Ref. [7]. The model thus fabricated was excited over a frequency range 20–40 Hz, and the relative motion between bolster and side-frame were obtained with a view to studying the stick-slip phenomenon. The following conclusions are drawn:

1. Stick-slip phenomenon appears consistently in the vicinity of 30 Hz (Figs. 7, 9–11) and less so at higher frequencies. At lower frequencies there are intervals, within the cycle of motion, during

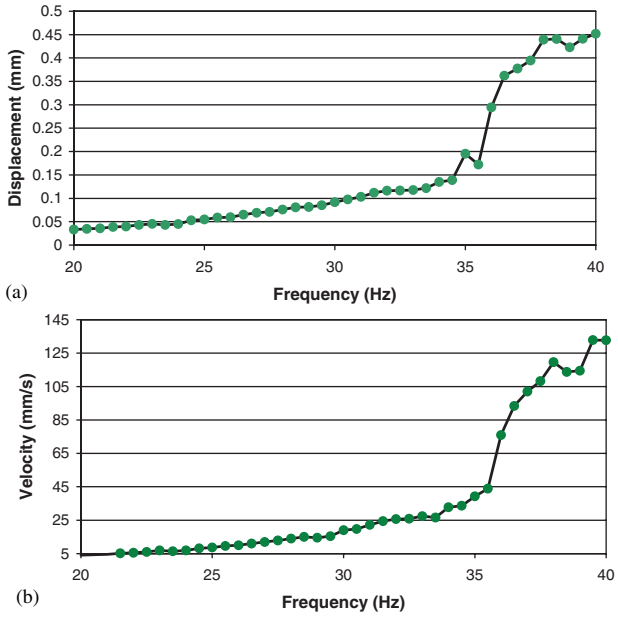

Fig. 13. Peak-to-peak response versus excitation frequency: (a) relative displacement, and (b) relative velocity.

which the inertial forces are insufficient to overcome static friction. This leads to stick events followed by slip when the inertial forces overcome static friction, i.e., stick-slip response.

2. Stick-slip phenomenon, is characterized by strong harmonic distortions (Table 3), which is indicative of increased quadratic and cubic nonlinearity effects. However, no trend emerges regarding the extent to which a particular harmonic contributes to the distortions.
3. Two types of stick-slip phenomena were observed. In type-A stick-slip, which is predominant at lower excitation frequencies, the relative velocity retains its direction after sticking (Figs. 7, 9–11) in contrast to type-B stick-slip (Figs. 11 and 12) which appears at higher excitation frequencies. Thus, at lower frequencies stick events occur well within the period of motion whereas at larger frequencies the stick events occur at the extremities of the cycle.
4. A transition from stick-slip to pure-slip appears between 30 and 40 Hz. It is characterized by a sharp increase in peak-to-peak response (Fig. 13). At higher frequencies, the inertial forces overcome static friction during the entire cycle of motion, thus leading to pure slip.

Future studies could involve online detection of permanent-stick/stick-slip followed by actuation/model parameter modification in order to obtain pure-slip, thus ensuring that dissipation is not curtailed.

References

[1] F. Xia, Modelling of Wedge Dampers in the Presence of Two-Dimensional Dry Friction, *Proceedings of the 17th IAVSD Symposium*, Lyngby, August 20–24, 2001, Supplement to *Vehicle System Dynamics*, Vol. 37, 2002, pp. 565–578.

[2] S. Shaw, On the dynamic response of a system with dry friction, *Journal of Sound and Vibration* 108 (2) (1986) 305–325.
[3] J.R. Anderson, A.A. Ferri, Behavior of a single-degree-of-freedom system with a generalized friction law, *Journal of Sound and Vibration* 140 (2) (1990) 287–304.
[4] S. Narayanan, K. Jayaraman, Chaotic vibration in a non-linear oscillator with Coulomb damping, *Journal of Sound and Vibration* 146 (1) (1991) 17–31.
[5] B.F. Feeny, F.C. Moon, Bifurcation sequences of a Coulomb friction oscillator, *Nonlinear Dynamics* 4 (1993) 25–37.
[6] N. Hinrichs, M. Oestreich, K. Popp, On the modelling of friction oscillators, *Journal of Sound and Vibration* 216 (3) (1998) 435–439.
[7] B. Kaiser, J.P. Cusumano, J.F. Gardner, Modeling and dynamics of friction wedge dampers in railroad freight trucks, *Vehicle System Dynamics* 38 (1) (2002) 55–82.